Computational and Structural Biotechnology Journal 23 (2024) 1689–1704

Contents lists available at ScienceDirect

Computational and Structural Biotechnology Journal

journal homepage: www.elsevier.com/locate/csbj

Research Article

Integration of single-nucleus and exosome RNA sequencing dissected inter-cellular communication and biomarkers in pancreatic ductal adenocarcinoma

Rong Tang [a,b,1], Zifeng Zhang [a,1], Jin Xu [a,b], Wei Wang [c,d], Qingcai Meng [a,b], Yuan Liu [b,e], Qiong Du [b,f], Chen Liang [a,b], Jie Hua [a,b], Bo Zhang [a,b], Xianjun Yu [a,b,*], Si Shi [c,d,**]

[a] Department of Pancreatic Surgery, Fudan University Shanghai Cancer Center, Shanghai, China
[b] Department of Oncology, Shanghai Medical College, Fudan University, Shanghai, China
[c] Shanghai Pancreatic Cancer Institute, Shanghai, China
[d] Pancreatic Cancer Institute, Fudan University, Shanghai, China
[e] Department of Endoscopy, Fudan University Shanghai Cancer Center, Shanghai, China
[f] Department of Pharmacy, Fudan University Shanghai Cancer Center, Shangai, China

ARTICLE INFO

Keywords:
Pancreatic cancer
MiRNA
Immune microenvironment
Exosome
Bioinformatics

ABSTRACT

Background: Mounting evidence underscores the importance of cell communication within the tumor microenvironment, which is pivotal in tumor proliferation, invasion, and metastasis. Exosomes play a crucial role in cell-to-cell communication. Although single-cell RNA sequencing (scRNA-seq) provides insights into individual cell transcriptional characteristics, it falls short of comprehensively capturing exosome-mediated intercellular communication.

Method: We analyzed Pancreatic Ductal Adenocarcinoma (PDAC) tissues, separating supernatant and precipitate for exosome purification and single-cell nucleus suspension. We then constructed Single-nucleus RNA sequencing (snRNA-seq) and small RNA-seq libraries from these components. Our bioinformatic analysis integrated these sequences with ligand-receptor analysis and public miRNA data to map the cell communication network.

Results: We established intercellular communication networks using bioinformatic analysis to track exosome miRNA effects and ligand-receptor pairs. Significantly, hsa-miR-1293 emerged as a prognostic biomarker for pancreatic cancer, linked to immune evasion, increased myeloid-derived suppressor cells, and poorer prognosis. Targeting this miRNA may enhance anti-tumor immunity and improve outcomes.

Conclusion: Our study offers a novel approach to constructing intercellular communication networks using snRNA-seq and exosome-small RNA sequencing. By integrating miRNA tracing with ligand-receptor analysis, we illuminate the complex interactions in the pancreatic cancer microenvironment, highlighting the pivotal role of miRNAs and identifying potential biomarkers and therapeutic targets.

1. Introduction

Intercellular communication plays a crucial role in the proliferation, invasion, and metastasis processes of tumors [1,41]. There is increasing evidence indicating the close cell-to-cell communication within the tumor microenvironment [2,14]. However, studying the communication between cells has always been a significant challenge. The application of single-cell RNA sequencing (scRNA-seq) allows us to predict cell-to-cell communication by analyzing the expression of ligand and receptor genes [10]. Nevertheless, cell communication takes various forms, and ligand-receptor analysis represents just one perspective in analyzing this complex phenomenon.

Exosomes, a specific type of extracellular vesicle with an average diameter of approximately 100 nanometers, are generated within cells and facilitate intercellular communication [12,24]. miRNAs are among the most important constituents of exosomes [9]. A growing body of

* Corresponding author at: Department of Pancreatic Surgery, Fudan University Shanghai Cancer Center, Shanghai, China.
** Corresponding author at: Shanghai Pancreatic Cancer Institute, Shanghai, China.
E-mail addresses: yuxianjun@fudan.edu.cn (X. Yu), shisi@fudanpci.org (S. Shi).
[1] The authors contributed equally to the manuscript.

https://doi.org/10.1016/j.csbj.2024.04.021
Received 15 January 2024; Received in revised form 1 April 2024; Accepted 7 April 2024
Available online 10 April 2024

research highlighted the biological effects of miRNAs within exosomes, originating from source cells and impacting target cells within the tumor microenvironment. For instance, Zhang et al. reported that cancer-associated fibroblasts can secrete miR-522, which suppresses ferroptosis and promotes acquired chemoresistance in gastric cancer [45]. Mechanistically, miRNAs could bind to the motif sequence of its target mRNA and trigger degradation or translation blockage [15,31]. The conservative motif information can serve as the foundation for constructing the miRNA-mRNA regulation network, contributing to prediction of intercellular communication. However, the origin and distribution of miRNAs in bulk tumor tissues are complex, making it challenging to systematically investigate the miRNA-target regulatory network at the intercellular level using traditional detection methods. The advent of scRNA-seq technologies has enabled the detection of primary miRNAs at single-cell resolution [16,37], allowing us to trace the source and target of miRNAs through the integration of exosome sequencing in a high-throughput manner.

Approximately 80% of patients with PDAC lost surgical opportunities due to rapid disease progression and late diagnosis. The expected five-year survival rate for patients with PDAC was below 10%, which reflected inadequate efficacy of current treatment modalities for PDAC [34]. Numerous studies have highlighted that targeting and disrupting the communication between cells is a crucial approach to inhibit the progression of PDAC. Therefore, recent studies have shifted focus to the communication and interactions among cells in the pancreatic cancer microenvironment[23,28,32]. Here, we integrated single-nucleus RNA and exosome small RNA sequencing from the same tumor tissue sample to infer cell-cell communication networks based on miRNA-target and ligand-receptor pairs in PDAC. Furthermore, we identified a novel miRNA biomarker with potential prognostic significance that may be involved in PDAC immune evasion.

2. Materials and methods

2.1. Sample processing for integrated sequencing

The “exo+snRNA-seq” technique uses frozen PDAC tissue (preserved in a −80 °C freezer) as the sample and performed by the company Oebiotch. First, RNA quality control is performed based on the sample conditions to detect whether RNA degradation has occurred during the sampling or collection process (RIN > 7). Next, a specific buffer is used to immerse the sample, followed by lysis and homogenization to release the cell nucleus and exosomes. The supernatant and precipitate are collected separately after centrifugation, and exosome purification and single-cell nucleus suspension preparation are performed. Exosome purification and RNA extraction are carried out using related reagents (QIAGEN) to ensure stable quality. The extracted miRNA is then processed for library preparation and sequencing using standard procedures. For the precipitate, the cell nucleus preparation lysis buffer is used for resuspension, and after purification and other steps, snRNA-seq is performed using the 10x Genomics protocol.

2.2. Single-nucleus RNA sequencing

The 10x Genomics platform uses microfluidic technology to encapsulate cells and Cell Barcode-labeled beads in droplets. The droplets containing cells are collected, and the cells are lysed within the droplets, allowing the mRNA within the cells to bind to the Cell Barcode on the beads and form Single Cell GEMs. Reverse transcription is then performed within the droplets to create cDNA libraries. The sample index on the library sequences is used to distinguish the origin of the target sequence. Cells with a gene count and UMI count within the range of the mean ± 2 times the standard deviation and a mitochondrial gene proportion of less than 10% are considered high-quality cells for downstream analysis.

The dimensionality reduction algorithms used in this project are Principal Components Analysis (PCA). The dimensionality reduction results based on PCA are visualized using t-distributed Stochastic Neighbor Embedding (t-SNE) for single-cell clustering. The clustering algorithm used is SNN, and the optimal cell subgroups are obtained. The definition of a marker gene is a gene that is highly expressed in the vast majority of cells in a specific cell population, but only expressed in a small proportion of cells in other cell populations, and the gene is significantly upregulated in this cell population compared to other cell populations. Annotations of cell combined strategies including autonomous (SingleR) and manual annotations (Literature-based). The bimodality test method is used to perform differential testing between the specified cell population and all other cell populations, thus screening for specific marker genes for each cell population. Other software used in the analyses were listed as follows: Cell Ranger (5.0.0), Seurat (3.1.1), Monocle2, Fastqc (0.11.7), Destiny (2.10.2), Scran (1.8.4) and MAGIC (1.2.1).

2.3. Observation of exosome samples using transmission electron microscopic

Exosome was extracted using ultracentrifugation separation, which can accurately and repeatedly obtain exosomes while minimizing co-purification of protein aggregates and other membrane particles .10 μL exosome sample was aspirated and added dropwise onto a copper mesh with precipitation for 1 min, and filter paper was used to suck off the floating liquid. Then, 10 μl uranium dioxide acetate was added dropwise onto a copper mesh and floating liquid was cleaned as well. Dry at room temperature for a few minutes. Electron microscopic examination and imaging were performed at 100 kv (Hitachi, HT-7700). The size of exosome sample was measured using a particle size analyzer (NanoFCM, N30E).

2.4. Preprocessing of small RNA sequencing data

The raw files obtained from high-throughput sequencing are converted into raw sequencing reads through base calling analysis. These raw sequencing reads, also known as RawData or RawReads, are then stored in the FASTQ file format, which contains the sequence information of the reads as well as their corresponding sequencing quality information. The raw FASTQ files need to be processed to remove adapter and primer sequences, followed by quality control and length filtering of the sequencing reads to select reliable ones. Then, the types (represented by "unique") and quantities (represented by "total") of small RNAs (sRNAs) are counted, and length distribution analysis is performed for miRNAs. Generally, the length of sRNAs falls within the range of 18–30 nt, and the peak of the length distribution can help identify the type of sRNA. For example, the length of miRNAs is typically concentrated in the range of 21–25 nt. Quality control methods and software were employed as described below: [1]. Cutadapt (version 1.14) was used to remove adapter sequences, and a custom script was used to filter out reads shorter than 15 nt or longer than 41 nt. Fastx_toolkit (version 0.0.13) was used to perform Q20 filtering to retain reads with Q20 scores of 80% or higher. NGSQCToolkit (version 2.3.3) was used to filter out reads containing N bases. The resulting high-quality reads were used for subsequent analysis and referred to as CleanReads. [4]. Fastx_toolkit (version 0.0.13) was used to count the number of unique reads in CleanReads. [5]. Bowtie software was used to align CleanReads sequences to the Rfam database (version 10.0), annotating rRNA, scRNA, Cis-reg, snRNA, and tRNA sequences, and filtering them out. Bowtie software was used to align Rfam-filtered reads to transcriptome sequences with a maximum of one base mismatch allowed. Reads with lengths between 15–26 nt in the alignment results were extracted and combined with reads that could not be aligned to the transcriptome sequence. These reads were used for subsequent analysis of known miRNA alignment and the prediction of new miRNAs. Bowtie software was used to align the transcriptome degradation fragment-filtered

sequences to the Repbase database to identify potential repetitive sequences. These sequences were filtered out and not used for subsequent analysis of known miRNA alignment and prediction of new miRNAs.

By aligning sequencing data to the miRBase database, known miRNAs can be identified and annotated. After filtering out repetitive sequences using the previous step, the filtered reads were aligned to the mature miRNA sequences in miRBase using the Bowtie software with a maximum of one base mismatch allowed. Sequences that were aligned were considered known miRNAs. These known miRNAs were used to quantify miRNA expression levels and for subsequent differential analysis.

2.5. Integrated analysis of snRNA-seq and exosome miRNA-seq

Based on the miRNA_primary_transcript gtf of miRBase, single-cell nuclear primary_miRNA analysis was performed to extract the miRNA expression and the marker miRNA of all cell types. Then, the correlation between exosomal miRNA expression and single-cell gene mRNA expression was analyzed using the Pearson correlation test. The detected cells were subjected to a random partitioning process, resulting in their division into three equal subsets. Similarly, the tissues designated for exosome miRNA detection were also evenly distributed into three identical portions. This meticulous allocation strategy adhered to the essential criterion of generating three distinct replicates for each of the two sample types involved in the study. Significant correlation was observed when the adjusted p-value was less than 0.05 and the absolute value of the Pearson coefficient (R) was greater than 0.8. The miRNA_v22 database was used to refer to the targets for every miRNA with potential interaction. Targets with an adjusted p-value of less than 0.05 and an R less than − 0.8 were considered as downstream of the miRNA with high confidence. The targets for hsa-miR-1293 were determined by the intersection of Diana_microt, PITA and TargetScan (TOP35%). Transcription factor list was derived from cisTarget (https://resources.aertslab.org/cistarget/). KEGG analysis was performed using the R package clusterProfiler (version 3.14.3). The source of miRNA was determined by single-cell nuclear primary_miRNA analysis, which identified the cells that expressed its primary RNA. We can determine the source of exosome miRNA by detecting which miRNAs are secreted into exosomes and by referring to the cell type-primary miRNA pairs. Network analysis was visualized using Cytoscape software (3.9.0). Some elements of ideograph were created with biorender (https://www.biorender.com/).

2.6. Bulk miRNA expression in samples of PDAC

The miRNA-Seq-miRNA expression quantification data was obtained from The Cancer Genome Atlas Program (TCGA) database (https://www.cancer.gov/ccg/access-data). Moreover, clinical follow-up data was also collected from the same database. Logrank test was performed to compare the survival differences (OS) between miR-1293-high and -low groups. The differentially expressed genes between miR-1293-high and -low PDACs were identified using DESeq2 algorithm.

3. In vitro experiments

3.1. Patient-derived Organoids

Human PDAC tissues from three patients were collected and digested into single-cell suspensions for organoid construction using PDAC dissociation reagent. The components of the reagent and procedures for digestion as well as culture media preparation were described in a previous publication [8]. Organoids were 3D cultured in Cultrex Path-Clear BME (R&D).

3.2. Co-culture system

Fibroblast cells in PDAC were separated and cultured as described in our previous study [38]. Peripheral blood was collected from PDAC patients before surgery with approval from the Clinical Research Ethics Committee of Fudan University Shanghai Cancer Center (FUSCC). To isolate T cells, PBMCs were subjected to magnetic cell sorting (Miltenyi Biotec, 130–096-535) to remove B cells, monocytes, natural killer cells, dendritic cells, early erythroid cells, platelets, and basophils. Human CD8 + T cells were then isolated from PBMCs through positive selection (Miltenyi Biotec, 130–045-201). T-cell activation was achieved using a T-Cell Activation/Expansion Kit (Miltenyi Biotec, 130–091-441). The T cells were cultured in RPMI 1640 (Gibco) supplemented with 20 IU/ml IL-2. A co-culture system of PDAC organoid, CAF and immune cells were conducted according to a previous study [13].

3.3. Oligonucleotides Transduction

RNA was extracted from fibroblast with indicated treatment using the SteadyPure Universal RNA Extraction Kit (AG21017). Reverse transcription was applied by C11027–2 riboSCRIPT Reverse Transcription Kit. The primers Bulge-LoopTM hsa-miR-1293 qPCR Primer Set (MQPS0000574–1-100) and Bulge-LoopTM U6 qPCR Primer Set (MQPS0000002–1-100) were used for qPCR. Hsa-miR-1293 and Has-miR-1291 mimic (Cat# miR10005883; Cat# miR20005881–1-5) and inhibitor (Cat# miR20005883, Cat# miR10005881–1-5) were used to upregulate or inhibit the hsa-miR-1293. The control group of transfections used equal miRNA mimic and / or inhibitor Negative control (Cat# miR1N0000001–1-5; Cat# miR2N0000001–1-5). All these products were provided by RIBOBIO. Fibroblast or panc-1 cells were transfected with miRNA mimic, inhibitor or control vector according to guidance of manufacturer's instructions. Briefly, cells were transfected approximately 80% confluence using Lipofectamine 3000 transfection reagent (Invitrogen) according to the manufacturer's protocol.

3.4. Cell Counting Kit-8 (CCK-8) and LDH release detection

For CCK-8 assay, the treated PDAC cells were seeded into 96-well plates at a concentration of 3×10^3/well. Then, 10 μL of CCK-8 assay solution (BIMAKE) was added and incubated in the dark for 2 h. The absorbance at 450 nm was measured every 24 h with a microplate reader (BioTek Instruments).

The LDH release assay was performed using an LDH Cytotoxicity Assay Kit (Cayman, 601170). "E" refers to signaling value for every well with indicated treatment, "S" refers to spontaneous release of well without treatment and M refers to the maximum release of LDH induced by triton. The percentage of relative LDH release was defined as (E-S)/(M-S).

3.5. Flowcytometry

Flowcytometry analysis was performed using the MoFlo XDP cytometer (Beckman Coulter, USA) and analyzed using FlowJo (V.10.6.1) or CytExpert. For xenograft tumors in mice, given the limitation of acquiring sufficient cells from certain smaller tumor masses, we aggregated tumor bulks within the same group and subsequently divided them into five random portions to ensure technical replication. The dissociation of xenograft tumors was conducted utilizing a mixture of Collagenase IV, hyaluronidase, and DNase I. This process was followed by filtration through a 70-micron pore-size filter. Our objective was to ascertain the proportion of CD3 + human T cells within xenograft tumors. To achieve this, cells were stained using the FITC Mouse Anti-Human CD3 antibody from BD. To assess PD-1 expression in T cells within a co-culture context, we employed anti-CD3 antibody in combination with anti-PD-1 (PerCP anti-human PD-1, Biolegend) staining (4 °C, 30 min). The protocols for flow cytometry procedures were

referenced from our previous publication [19].

3.6. Fluorescence in situ hybridization (FISH) assay and PDAC tissue slices

The protocol for FISH we conducted was referred to our previous study [30]. Briefly, the experiment involved tissue fixation, dehydration, and sectioning, followed by a series of hybridization, washing, and staining steps. Pre-hybridization, hybridization with probes, and signal hybridization were conducted in a humidity chamber, with washes in SSC buffers at varying temperatures. Finally, cell nuclei were stained with DAPI, and microscopic examination and photography were conducted using a fluorescence microscope (NIKON ECLIPSE CI;) with different excitation and emission wavelengths for each fluorophore. The expression level of miR-1293 in PDAC tissues was evaluated by FISH in PDAC tissues from 176 patients who were diagnosed with PDAC at the FUSCC between 2012 to 2018. Differential expression analysis of miR-1293 between cancerous and normal regions was performed using 57 pairs of tumor and adjacent pancreatic tissue slices. All samples were evaluated by two independent pathologists. The intensity of miR-1293 staining was scored as follows: 0, no staining; 1, low staining; and 2, high staining. The percentage of positively stained cells was scored as follows: 0, 0% (no stained cells); 1, 1 ~ 24%; 2, 25 ~ 49%; 3, 50 ~ 74%; and 4, 75 ~ 100%. The final score was calculated by multiplying the scores for the staining intensity and the percentage of positively stained cells. Subsequently, the samples were divided into two groups: the low expression group (score 0–3) and the high expression group (score 4–8). The FISH probe of miR-1293 was purchased from Vazyme Biotech Co, Ltd (5′-GCACAAATCTCCAGACCACCCA-3′).

3.7. Targeted metabolome

Samples were taken out at − 80 °C, slowly thawed at 4 °C, and then 0.5 ml of a methanol-acetonitrile-water solution (2:2:1, v/v) was added. Next, 10 μL of SUCCINIC ACID-D6 internal standard (10 mMol/L) was added, followed by 60 s of vortexing and 30 min of low-temperature sonication, repeated twice. The samples were then left at − 20 °C for 1 h to precipitate proteins. After centrifugation at 14,000 rcf at 4 °C for 20 min, the supernatant was collected, freeze-dried, and stored at − 80 °C.

Chromatography Conditions were listed as follows: Samples were separated using an Agilent 1290 Infinity LC Ultra-High Performance Liquid Chromatography system. The samples were kept in an automatic sampler at 4 °C, the column temperature was set at 35 °C, and the mobile phase A consisted of a 50 mM ammonium acetate aqueous solution with 1.2% ammonium hydroxide, while mobile phase B consisted of a 1% acetonitrile solution of acetone. The flow rate was 300 μL/min, and the injection volume was 2 μL. In the sample queue, a QC sample was set at regular intervals to monitor and evaluate system stability and repeatability. A standard mixture of target substances was also included in the sample queue for calibration of chromatographic retention times. Mass spectrometry analysis was performed using a 5500 QTRAP mass spectrometer (SCIEX) in negative ion mode. The ESI source conditions for the 5500 QTRAP were as follows: source temperature 450 °C, Ion Source Gas1 (Gas1): 45, Ion Source Gas2 (Gas2): 45, Curtain gas (CUR): 30, ion Spray Voltage Floating (ISVF) − 4500 V. The Multiquant 3.0.2 software was used to extract peak areas and retention times from the chromatograms. Chromatographic retention times were corrected using standards of target substances for metabolite identification. Principal Component Analysis (PCA) and Partial Least Squares Discriminant Analysis (PLSDA) were performed to visualize the difference of metabolites landscape between two groups.

3.8. Luciferase reporter assay

The Dual-Luciferase Reporter Assay System (Promega) was used to detect firefly and renilla luciferase from the pmirGLO-FOXO3 plasmids and pmirGLO-FOXO3 Mut (mutated site) plasmid in mimic and empty vector miR-1293-transfected cells. These plasmids were synthesized by RIBOBIO. Twenty-four hours following transduction with recombinant plasmids using Lipofectamine 3000, the cells were rinsed with PBS in preparation for cell lysis. The cells were ensured to be no more than 95% confluent at the time of lysis. After lysis, firefly and renilla luciferase activity were sequentially measured according to the instruction of manufacturer. The luciferase activity (firefly luciferase / renilla luciferase) was normalized to the group with empty vector.

3.9. Western blotting analysis

Western blotting was performed as described in our previous study [39]. In brief, proteins were extracted from PDAC cells using RIPA buffer supplemented with protease and phosphatase inhibitors. For exosome samples: Thaw the exosomes at 37 °C and rapidly add 5 × RIPA lysis buffer. After mixing, lyse on ice for 30 min, mixing periodically. Then, calculate the protein concentration of the sample based on the standard curve with BCA methods. Equal amounts of protein were separated on 10% SDS-PAGE gels and transferred onto PVDF membranes (Millipore), which were then blocked for 2 h in 5% skim milk. The membranes were subsequently probed with primary antibodies targeting the following proteins: FOXO3A (Proteintech, 66428–1-Ig), TSG101 (Abcam, ab125011), Calnexin (SAB, 12186), CD86 (41779), CD9 (Boster, BM4212) and β-actin (66009–1-lg, Proteintech). The membranes were then incubated with appropriate secondary antibodies (Proteintech, China) for 1 h. After three washes, the target proteins were visualized using enhanced chemiluminescence (ECL) reagent (Millipore, MA, USA). β-actin served as the loading control in this study.

3.10. Animal studies

NPSG mice were housed in ventilated caging units in the Shanghai Cancer Center Specific Pathogen Free (SPF) facility with standard housing and husbandry and free access to food and water. To generate immunologically humanized patient-derived xenografts (PDXs), we first established a PDX model following the procedures outlined in our previous study [18]. Briefly, every surgically resected PDAC sample divided into five equal blocks of approximately 10 mm^3 each for subcutaneous transplantation into the flanks of female NPSG mice (6–8 weeks old). Meanwhile, 5×10^5 CAFs with mimics of has-miR-1293 or control vector were co-transplanted with tumor blocks. A week later, 2×10^7 PBMC isolated human PBMCs were resuspended in 500 μL PBS and intravenously injected into PDX mice. Then, mice (n = 5 for each group) were treated with Durvalumab intraperitoneally at the dosage of 0.5 mg/kg twice a week. Tumor volume was measured every 7 days using calipers and calculated with the formula: volume = 0.5 × length×width2.

3.11. Statistical analysis

To compare continuous variables, we conducted either a paired or unpaired t-test based on whether the two groups were matched. To assess the overall survival duration of patients, we employed the log-rank test. The association between two sets of data was evaluated using Pearson correlation. In all experiments, statistical significance was determined at a threshold of $P < 0.05$. All graphs and statistical computations for the experimental data were generated using Prism 9.0.0 (GraphPad).

4. Results

4.1. snRNA-seq revealed primary miRNA expression in single-cell resolution

We obtained both snRNA-seq and small RNA-seq libraries from the same bulk of two tumor tissues, following the workflow outlined in Fig. 1A. Human pancreatic cancer tissues were surgically resected, dissociated, and homogenized before being centrifuged. Post-centrifugation, the upper layer contained the supernatant while the lower layer held the precipitate. The supernatant was used for exosome purification and small RNA sequencing, while the precipitate was employed for snRNA-seq. After quality control measures eliminated ineligible cells, 8841 cells were analyzed using the Seurat pipeline. We initially annotated three major cell types: epithelial cells, stromal cells, and immune cells (Fig. 1B). As anticipated, epithelial cells were the most abundant cell type in pancreatic cancer tissue (61.1%) according to snRNA-seq data (Fig. S1A). This percentage was significantly higher than that observed in traditional scRNA-seq, as demonstrated by a large scRNA-seq-based cohort (Fig. S1B-C). We further annotated six distinct cell subclusters, with PDAC cells being divided into two subtypes (Fig. 1C). Differential expression analysis was performed for ductal cell-

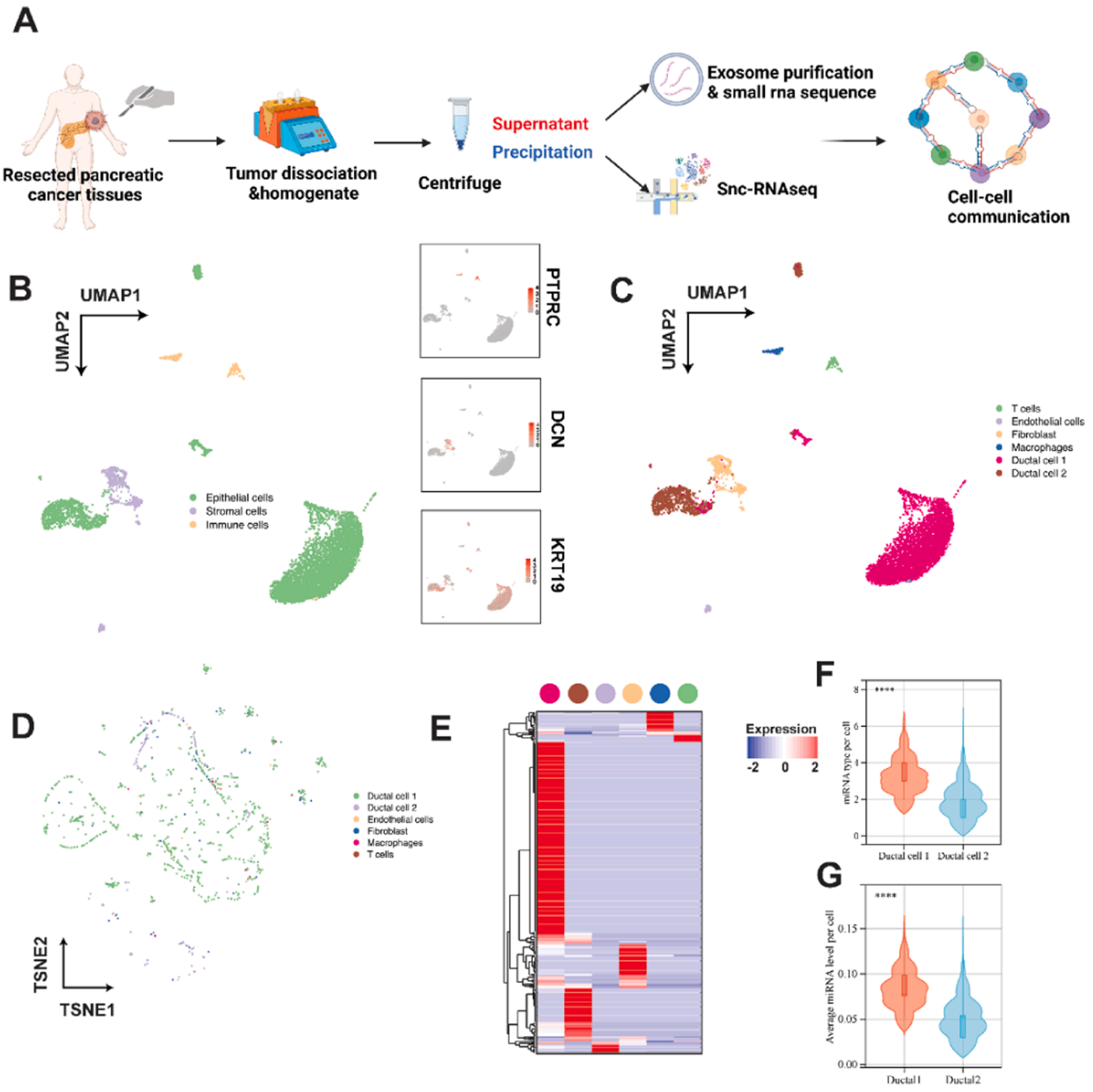

Fig. 1. Analysis of single-cell RNA sequencing in pancreatic cancer tissues. (A) Workflow of snRNA-seq and small RNA-seq library preparation from surgically resected human pancreatic cancer tissues. (B) UMAP plot showing three major cell types: epithelial cells, stromal cells, and immune cells. (C) Further annotation for cell subclusters in UMAP approach. (D) t-SNE analysis based on primary miRNA expression. (E) Heatmap showed cell type-specific primary miRNA expression. (F-G) Violin plot showed increased abundance and expression of primary miRNAs in ductal cell type 1.

1 and − 2 clusters. Genes upregulated in ductal cell-1 (logfc>2, adjP<0.05) were enriched in cAMP signaling, Ras signaling, and other pathways, while those upregulated in ductal cell-2 were enriched in metabolic pathways, such as oxidative phosphorylation (Fig. S1D-E). Although cells displayed a scattered distribution when compared by cell marker dimensions (Fig. 1D), we also observed that many primary miRNAs exhibited cell type-specific expression, of which most primary miRNAs were detected in ductal and fibroblast cells (Fig. 1E). Notably, ductal cell-1exhibited the higher abundance and level of primary miRNAs compared with ductal cell-2 counterparts (Fig. 1F-G).

4.2. Construction of cell-cell communication networks via miRNA tracing and miRNA-target effect

As previously described, we obtained the supernatant from dissociated tumor tissues. We then extracted exosomes from the supernatant using ultracentrifugation separation (Fig. 2A and Fig. S2A). The size and concentration of the exosomes were measured to ensure a successful extraction process and confirm that the exosomes were of high quality (Fig. 2B-C and Fig. S2B-C). Western blot further validated the identity and purity of exosomes (Fig. S2D). The distribution of miRNA lengths was plotted in curves for various samples (Fig. S2E). We defined downstream cells as those that receive exosome miRNAs, which interfere with the target mRNA containing corresponding motifs in these cells (Fig. 2D). To achieve this, we analyzed the quantitative correlation between exosome miRNA expression and single-cell mRNA expression. Using a threshold of $r < -0.8$ and an adjusted P value < 0.05, we identified numerous negatively correlated miRNA-mRNA pairs in each cell type. Additionally, we constrained the miRNA-mRNA pairs to those with motif matches. The results revealed that the ductal-2 celltype had the highest number of miRNA-mRNA pairs with negative expression and motif matches. This finding suggests that the ductal-2 cell is the primary downstream cell type that can be widely regulated by exosome miRNAs (Fig. 2E).

We defined upstream cells as those that release corresponding miRNAs into the extracellular microenvironment via exosomes. These miRNAs are then received by downstream cells and exert inhibitory effects on target genes (Fig. 2F). To accomplish this, we intersected exosome miRNAs with primary miRNAs detected in snRNA-seq. The intersected miRNAs were secreted into exosomes by specific cell types. Interestingly, we found that the ductal-1 cell type had the most abundant secretion of miRNAs, suggesting it as the major source of miRNA secretion (Fig. 2G). T cells and macrophages exhibited less miRNA communication with other cells, indicating that miRNA regulation may play a less role in immune cells. Conversely, fibroblasts appeared to be active both as exosome RNA sources and receivers.

Numerous studies have revealed that miRNAs play a significant role in endothelial cells by regulating their proliferation and migration, which are involved in angiogenesis and inflammation [11,21,42,44]. For cancerous diseases, endothelial cells-derived miRNAs exerted important role in tumor drug resistance, growth, and metastasis [25,26,43]. Here, we found that endothelial cells were the third-largest source of miRNAs among all identified cell types. However, given that the relatively lower number of miRNA-target pairs discovered, endothelial cells themselves may be less regulated by exosome-miRNAs. Next, we constructed an intercellular communication network by depicting upstream cells, exosome-miRNAs, and downstream cells (Fig. 2H). Exosome-derived hsa-miR-1248 was predicted to originate from both ductal 1 and 2 cells based on the network, suggesting that hsa-miR-1248 is conserved in the pancreatic ductal structure during differentiation. Fibroblast, endothelial, and ductal 2 cells themselves were potential downstream cells via the hsa-miR-1248-PIP5K1A pair. Similarly, hsa-miR-1267 was also secreted by both ductal 1 and 2 cells and projected to influence downstream fibroblast cells by interfering with ITGA6.

Notably, hsa-miR-4647, originating from ductal 1, ductal 2, and fibroblast cells, could exert effects on all downstream cells by targeting ATF7, CCSER2, RELL1, SSBP2, and USP47. This finding suggests a potential role of hsa-miR-4647 as a messenger in the tumor microenvironment. A recent study revealed hsa-miR-4647 was one of two significantly upregulated miRNAs in gallbladder carcinoma and associated with patients' unfavorable prognosis [36], suggesting hsa-miR-4647 could be a promising target for developing novel treatment modality for gallbladder carcinoma.

4.3. Enrichment analyses for gene targets in cells when served as upstream and downstream of exosome-miRNAs

We identified specific targets for exosome-miRNAs potentially originating from ductal-1 and − 2 cells through motif matching (Fig. 3A). Enrichment analyses revealed that gene targets of ductal-1-related miRNAs were primarily involved in pathways related to cancer, Ras signaling, HIF signaling, and Hippo signaling. In contrast, gene targets of ductal-2-related miRNAs were more enriched in pathways associated with normal pancreatic functions, such as insulin secretion (Fig. 3B-C). Additionally, we performed enrichment analysis for gene targets when cells served as downstream recipients of exosome-miRNAs. This analysis showed that exosome-miRNAs might regulate gene targets involved in ferroptosis in ductal-1 cells, while modulating adherens junctions and ErbB signaling pathways in ductal-2 cells (Fig. S3A-B). Furthermore, it was hypothesized that T cell-derived exosome-miRNAs regulate Hippo signaling, while the exosome-miRNAs they receive regulate ferroptosis, pyrimidine metabolism, and inositol metabolism (Fig. 3D and Fig. S3C). For fibroblasts, their secreted exosome-miRNAs may regulate genes involved in MAPK signaling and PI3K-Akt signaling, which have been widely reported as oncogenic pathways in cancer [33,35,46] (Fig. 3E). When fibroblasts served as recipients for exosome-miRNAs, pathways including cell adhesion molecules and Wnt signaling were potentially regulated (Fig. 3F). In contrast, when endothelial cells served as downstream recipients, MAPK signaling was enriched in target genes for exosome-miRNAs, while Wnt signaling was enriched when endothelial cells served as both upstream and downstream components (Fig. S3D-E). The exosome-miRNAs that macrophages most likely received may regulate genes involved in ferroptosis and pyrimidine metabolism, while the exosome-miRNAs they released may regulate genes related to the sulfur relay system and dopaminergic synapses (Fig. S3F-G).

4.4. Construction of cell-cell communication networks via miRNA-target effect and ligand-receptor pair analysis

Ligand-receptor pair-based analysis has been widely applied to uncover cell-cell communication in various fields, particularly in the tumor microenvironment [1,10,14]. We utilized the CellChat algorithm to investigate intercellular communication among the identified cells. The strength and number of interactions have been illustrated using a circus plot, which revealed abundant interactions between each cell type, particularly between fibroblasts and ductal 1 cell (Fig. 4A-B). In the CellChat pipeline, incoming signaling represents the influence of signal transduction received by a cell from other cells, while outgoing signaling signifies the influence of signal transduction generated by a cell on other cells. Overall, fibroblasts exhibited the most abundant outgoing signaling patterns compared to other cell types, especially including collagen, laminin, NRXN, and ncWNT. In contrast, ductal 1 cell was the primary recipients of incoming signaling, encompassing collagen, laminin, FN1, VEGF, CD99, CDH, and others (Fig. 4C). The scatter plot based on incoming and outgoing interactions supported these findings and further demonstrated that ductal 2 cells had limited interactions with other cells via ligands and receptors (Fig. 4D). To cluster cells and communication patterns, cophenetic and silhouette methods were applied to determine the optimal number of clusters (Fig. 4E and Fig. S4A). For both incoming and outgoing signaling, we identified three clusters as the optimal choice for clustering. Interestingly, stromal cells

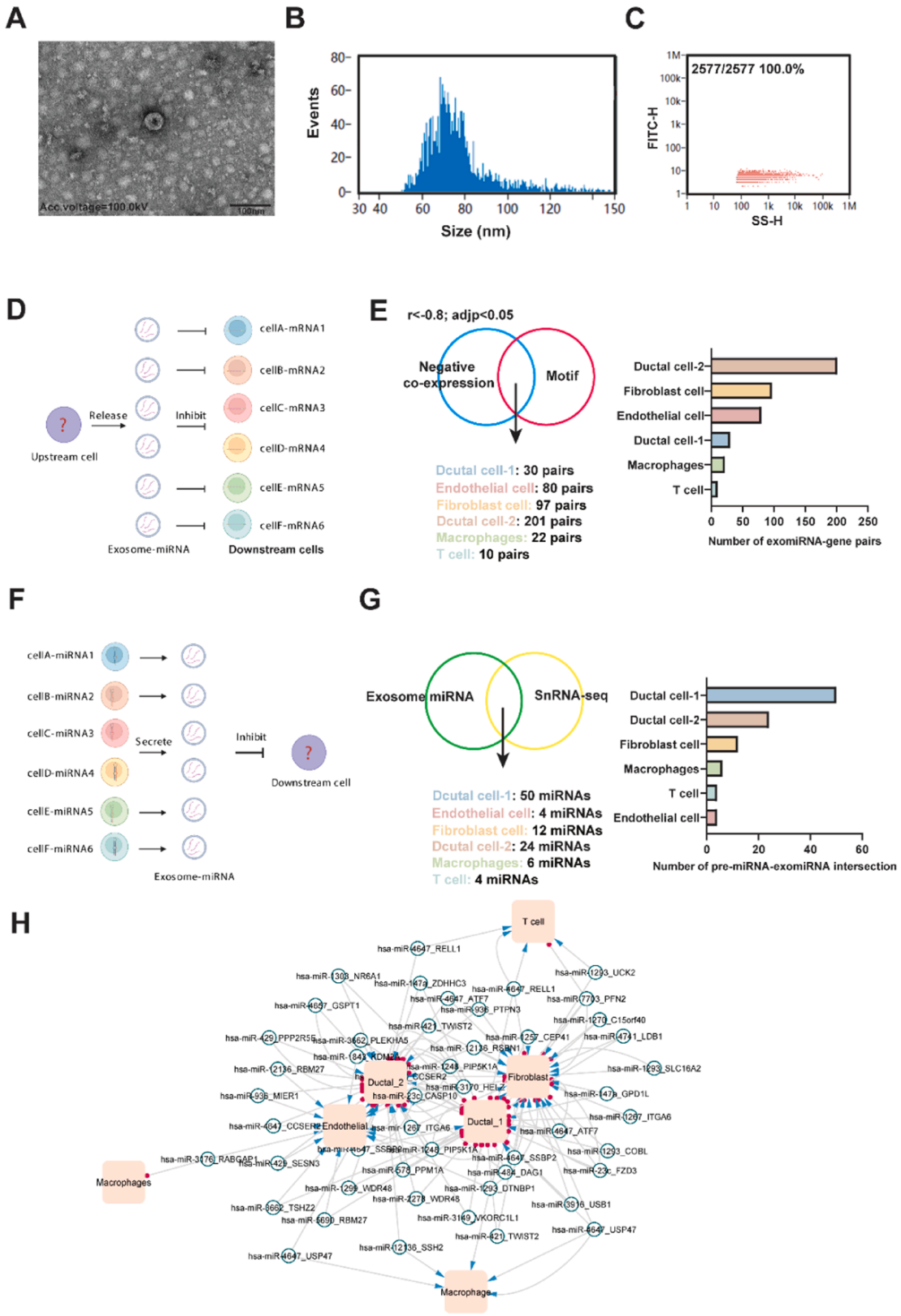

Fig. 2. Construction of intercellular communication networks via miRNA tracing and miRNA-target effect. (A) Transmission electron microscopic image of exosome extracted from the supernatant of dissociated tumor tissues (sample 1). (B-C) Measurement of particle size for Exosome. (D) Schematic of defining downstream cells based on exosome miRNA expression and single-cell level mRNA expression. (E) miRNA-mRNA pairs with negative expression and motif match in each cell type. (F) Schematic of defining upstream cells based on miRNA secretion. (G) Tracing the source of exosome miRNA by intersection with primary miRNAs detected using snRNA-seq. (H) Network presented the upstream and downstream of exosome-miRNAs to showcase cell-cell communication.

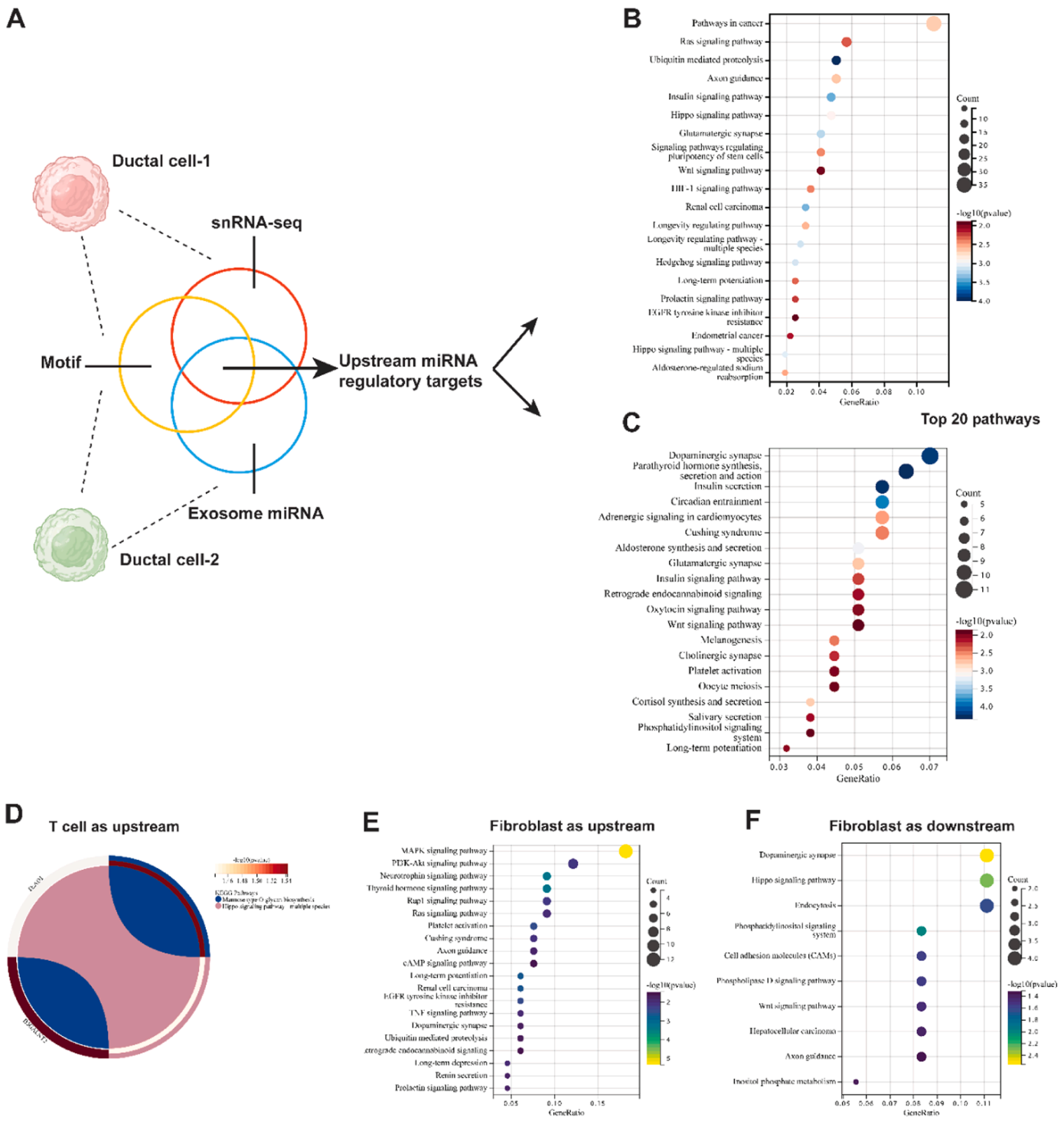

Fig. 3. The pathway enrichment analysis for exosome-miRNA target gene analysis. (A) Motif match detection of specific targets for exosome-miRNAs in ductal 1 and 2 cells. (B-C) Pathway enrichment analysis of gene targets for ductal 1 and 2-related miRNAs. (D) T cell-derived exosome-miRNA regulation of Hippo signaling and the exosome-miRNA it received regulating ferroptosis, pyrimidine, and inositol metabolism. (E) Fibroblast-secreted exosome-miRNA regulation of MAPK and PI3K-Akt signaling pathways. (F) Exosome-miRNA regulation of cell adhesion molecules and Wnt signaling in fibroblasts when serving as a receiver.

(fibroblasts and endothelial cells), immune cells (T cells and macrophages), and pancreatic ductal cells (ductal 1 and ductal 2) were respectively clustered based on outgoing signaling (Fig. 4F). Clustering for communicated ligand-receptor pairs also revealed three patterns (Fig. S4B). The outgoing communication patterns of secreting cells are shown in Fig. S4C. Overall, the communication patterns for incoming and outgoing signaling exhibited several similarities. For instance, TGF-b, MHC-II, CADM, CD45, and GRN were conservatively clustered, while FN1 and collagen formed another conservative cluster (Fig. S4D-E). Furthermore, the patterns of signaling interactions received by targeted cells from other cells were visualized (Fig. S4F). Next, we established cis- and trans-regulatory networks by combining miRNA-target and ligand-receptor information. First, we discovered 442 significant ligand-receptor pairs using cell-chat algorithm. Among 1129 genes either ligand or receptor, we further detected 95 motif-matched miRNA-target pairs for the construction of cis- and trans- regulation

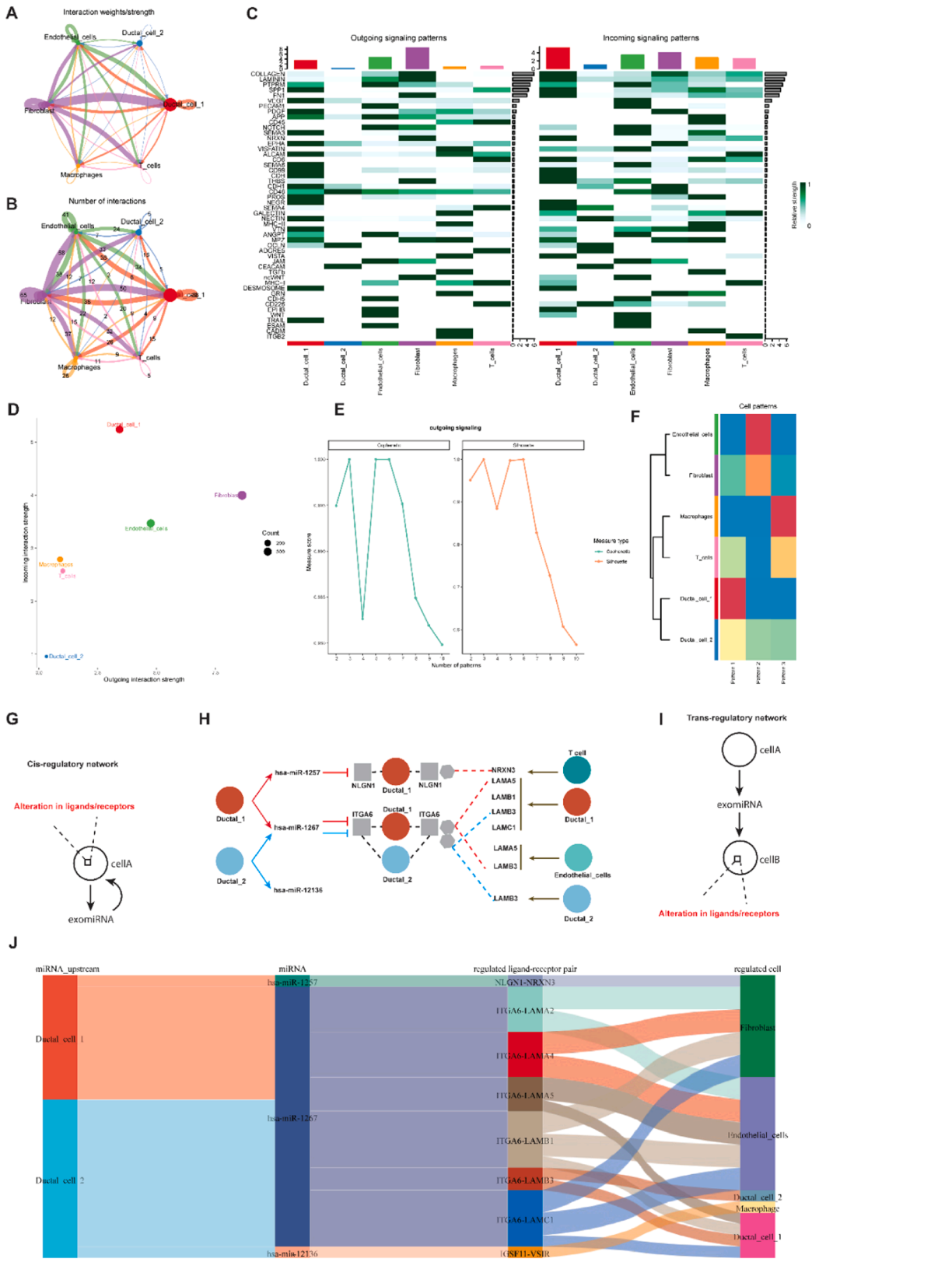

Fig. 4. Ligand-receptor pair analysis for cell-cell communication networks. (A-B) Circus plot showing the strength and number of interactions between each cell type, respectively. (C) Heatmap showing the detailed interactions between among cells in terms of incoming and outgoing signaling patterns. (D) Scatter plot showed abundant outgoing signaling patterns in fibroblast cells and incoming signaling patterns in ductal 1 cells. (E) Cophenetic and Sihouette analysis determined the cluster number for outgoing signaling patterns. (F) Clustering of cells based on outgoing signaling patterns. (G) The schematic of Cis-regulatory network. (H) Construction of cis-regulatory network by combining miRNA-target and ligand-receptor information. (I) The schematic of Trans-regulatory network. (J) Construction of trans-regulatory network by combining miRNA-target and ligand-receptor information.

network. Cis-regulation is defined as cell A secreting exosome-miRNAs that may act on cell A's ligands/receptors (Fig. 4G). For example, ductal 1 cells may secrete exosome-miRNAs containing hsa-mir-1257 and hsa-mir-1267, which could potentially downregulate the expression of receptors NLGN1 and ITGA6 on the ductal 1 cells themselves (Fig. 4H). In this context, ductal 1 cell would become insensitive to NRXN3 from fibroblasts and LAMs from endothelial cells, other ductal cells, and fibroblasts. Trans-regulation is defined as cell A secreting exosome-miRNAs that may act on cell B's ligands/receptors (Fig. 4I). Here, we demonstrated that ductal cell-2-derived hsa-mir-12136 might directly downregulate IGSF11-VSIR interaction, which is the receptor on ductal 1 cell (Fig. 4J).

4.5. Identify the role of prognosis-relevant exosome-miRNAs in immune microenvironment of PDAC

To investigate the expression of exosome-miRNAs and their association with the prognosis of PDAC patients, we analyzed transcriptome data and clinical outcomes of the PDAC cohort in TCGA. By intersecting the exosome-miRNA data we obtained with the TCGA miRNA sequencing data, we identified 281 miRNAs that were common to both datasets (Fig. 5A). To determine the prognostic value of these miRNAs, we performed survival analysis using batched univariate COX regression and identified 25 miRNAs that were significantly associated with patient survival, with 12 miRNAs showing a survival benefit and 13 miRNAs associated with worse survival time (Fig. 5B). By further intersecting these miRNAs with the primary miRNAs detected using snRNA-seq in PDAC, we identified five miRNAs that were prognostic biomarkers, with four of them potentially secreted by ductal-1 cells and one (hsa-miR-1293) predominantly traced to fibroblasts (Fig. 5C). Upon re-examining the miRNA expression matrix, we found that 98.9%, 88.0%, and 70.5% of PDAC samples did not express hsa-mir-1257, hsa-mir-3149, and hsa-mir-578, respectively. This high percentage of missing values could significantly reduce the reliability of the association between miRNAs and patients' prognosis. Hence, we focused on hsa-mir-1291 and hsa-miR-1293. Our results confirmed that higher expression of hsa-miR-1293 was associated with a worse prognosis for PDAC patients (Fig. 5D). In contrast, there was no significant trend indicating that hsa-mir-1291 expression was associated with PDAC patients' survival time, both for the median value cutoff and the optimal cutoff value determined by the maxstat algorithm (Fig. S4G-H). The ROC curve also demonstrated that hsa-miR-1293 had high accuracy for predicting the prognosis of PDAC (Fig. 5E). In previous sections, we demonstrated that exosome miRNAs play a crucial role in cell-to-cell communication within the tumor microenvironment. To further investigate the association between miRNA expression and immune cell infiltrates, we estimated the relative abundance of tumor-infiltrating immune cells using the CIBERSORT algorithm. Our correlational analyses revealed that CD8 + T cells, a major anti-tumor component, were negatively correlated with hsa-miR-1293 expression, but not with hsa-mir-1291 (Fig. 5F). This finding was consistent across various algorithms for immune cell infiltration estimation, including classic and ABS CIBERSORT (Fig. 5G). In addition, we found a strong positive correlation between hsa-miR-1293 expression and the score of myeloid-derived suppressor cells (MDSCs), which are known to inhibit anti-tumor immunity (Fig. 5H). Furthermore, we compared the level of immune regulators in PDAC groups with high and low expression of hsa-miR-1293 (Fig. 5I). We observed that VEGFA, but not VEGFB, was significantly upregulated in PDAC samples with overexpression of hsa-miR-1293, suggesting that targeting VEGFA could be a valuable strategy for PDAC patients with high hsa-miR-1293 expression. Numerous genomic parameters have been reported to be associated with the immune microenvironment in PDAC. For instance, tumor mutation burden has emerged as a popular biomarker for predicting the efficacy of immunotherapy in many cancers and has been found to be independent of T cell-inflamed gene expression profiles[5,29]. Our findings suggest that hsa-miR-1293 expression is highly correlated with high tumor mutation burden (TMB), microsatellite instability (MSI), and neoantigen levels, indicating that inhibiting hsa-miR-1293 expression may enhance the efficacy of immunotherapy (Fig. 5J). In addition to genetic biomarkers, transcriptome-based molecular subtyping has emerged as an effective approach to distinguish cancer patients with distinct molecular characteristics and guide different clinical treatments. For PDAC patients, three molecular subtypes have been previously identified, including the Moffitt subtype, Collison subtype, and Bailey subtype. We calculated the distribution of these subtypes in PDAC patients with high and low miR-1293 expression and found no significant differences in the percentages of Moffitt and Collison subtypes between the two groups (Fig. 5K). However, we observed that more immunogenic subtypes were present in the miR-1293-low group, while progenitor and squamous subtypes showed downregulated percentages in the same group (Fig. 5K).

4.6. Targeting miR-1293 in CAF boost T cell-mediated anti-tumor immunity

Recently, Koikawa et al. introduced a co-culture system of pancreatic cancer organoid, CAFs and immune cells [13]. In this study, we used a co-culture system to investigate the impact of miR-1293 expression on T cell anti-tumor function (Fig. 6A). We transfected CAFs with miR-1293 mimic and inhibitor to overexpress or inhibit miR-1293 expression, respectively, followed by co-cultured the CAFs with pancreatic cancer organoids and activated T cells. PD-1 upregulation in tumor-infiltrating T cells is an important mechanism by which tumor cells evade immune cell attack. Therefore, we performed flow cytometry to measure PD-1 expression in T cells in each group. Our results showed that T cells co-cultured with miR-1293-mimic CAFs had the highest PD-1 expression, while inhibition of miR-1293 in CAFs decreased PD-1 expression in co-cultured T cells (Fig. 6B-C and Fig. S4I). Next, we investigated whether miR-1293 regulation in CAFs would affect T cell-mediated tumor killing. T cell-mediated tumor killing primarily occurs through apoptosis. To label apoptotic organoids, we used a green-fluorescent caspase 3/7 probe reagent and found that the co-culture system with miR-1293-overexpressing CAFs had less apoptotic organoids with collapsed structures, while organoids co-cultured with wild-type (WT) CAFs and CAFs with miR-1293 inhibitor showed higher apoptotic signals (Fig. 6D). To quantify the altered killing ability of co-cultured T cells, we transferred T cells from different groups into a new co-culture system with pancreatic cell lines. LDH release assay confirmed that T cell killing ability was compromised after co-cultured with CAFs overexpressing miR-1293, while the opposite effect was observed when co-cultured with CAFs with miR-1293 inhibition but not with miR-1291 (Fig. 6E and Fig. S4J). In addition, our data indicated that miR-1293 potentially regulates multiple gene targets in pancreatic ductal cells, suggesting that miR-1293 may influence the progression of PDAC cells. Consequently, we directly overexpressed or inhibited miR-1293 in a PDAC cell line to assess its impact on cell proliferation. The results demonstrated that miR-1293 mimic moderately promoted cell proliferation, while the miR-1293 inhibitor significantly reduced cell proliferation (Fig. 6F).

In order to delve into the potential mechanisms underlying the relationship between miR-1293, immune evasion, and a moderate increase in cell proliferation, we conducted a gene enrichment analysis to elucidate the molecular distinctions between miR-1293-high and -low PDACs (Fig. 6G). Notably, the KEGG analysis unveiled that the DEGs between the two PDAC groups were intricately linked to the glycolysis/gluconeogenesis pathway. Specifically, key glycolytic enzymes, including ENO1, GAPDH, ALDOA, and HK2, exhibited significant upregulation in miR-1293-high PDAC samples (Fig. 6H). To further validate these findings at the metabolome level, we scrutinized the energy metabolism metabolites in co-cultures of PDAC organoids and CAFs transfected with mimic-1293 or mimic-NC (Fig. 6I). Both PCA and

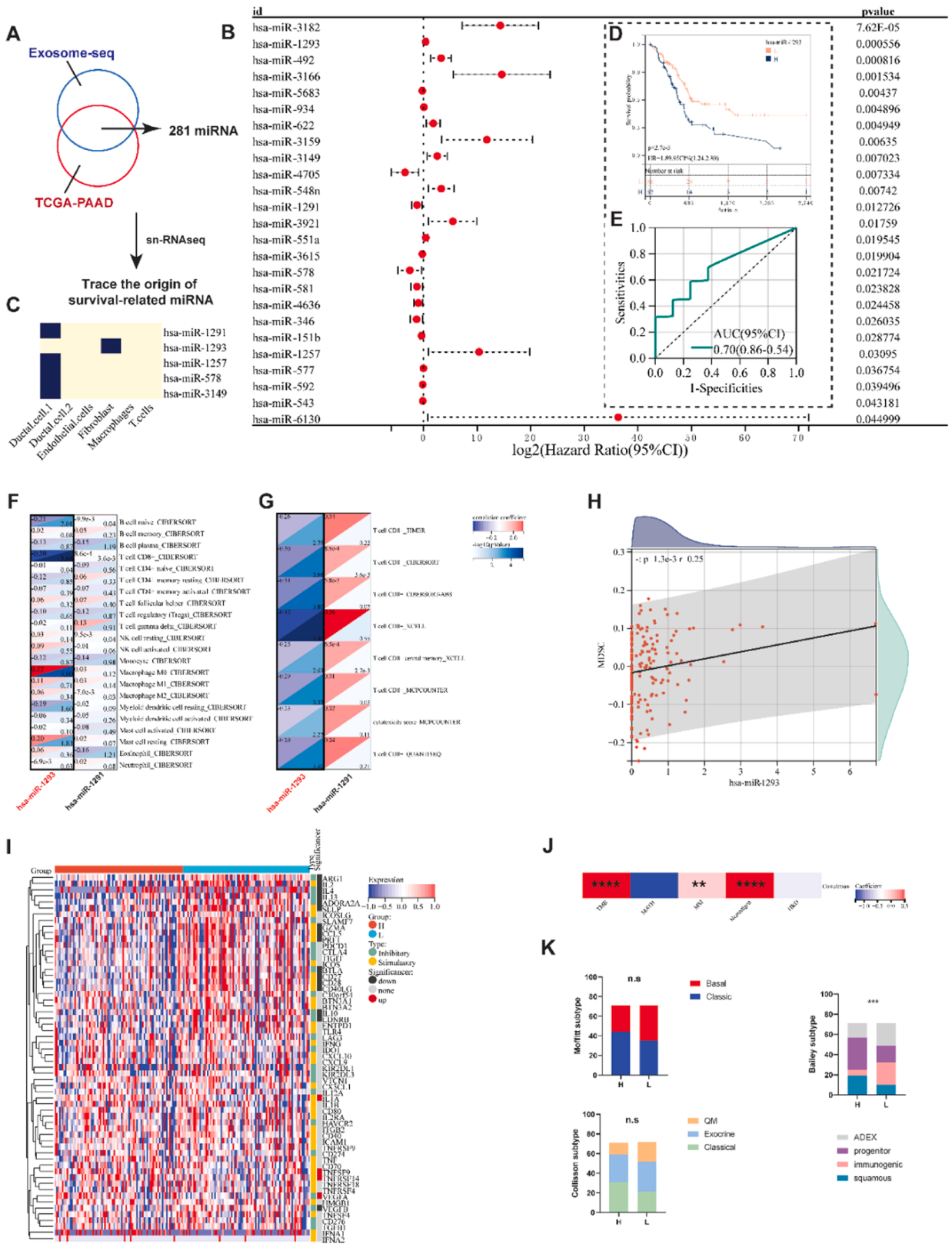

Fig. 5. Prognostic relevance of exosome-miRNAs in immune microenvironment of pancreatic cancer. (A) Overlap of exosome-miRNAs detected in this study and TCGA miRNA sequencing data. (B) Survival analysis of prognosis-related miRNAs by univariate COX regression. (C) Prognostic miRNAs intersected with primary miRNAs detected in snRNA-seq. (D) Kaplan-Meier curve showing pancreatic cancer patients based on hsa-mir-1291 and hsa-miR-1293 expression (Log-rank test). (E) ROC curve for hsa-miR-1293 in predicting prognosis. (F-G) Correlation between CD8 + T cell infiltration and hsa-mir-1291 and hsa-miR-1293 expression. (H) Positive correlation between hsa-miR-1293 expression and MDSC score. (I) Expression of immune regulators in high and low hsa-miR-1293 expression groups. (J) Correlation between hsa-miR-1293 expression and genomic parameters. (K) The distribution of hsa-miR-1293-high and -low PDAC samples among different molecular subtypes.

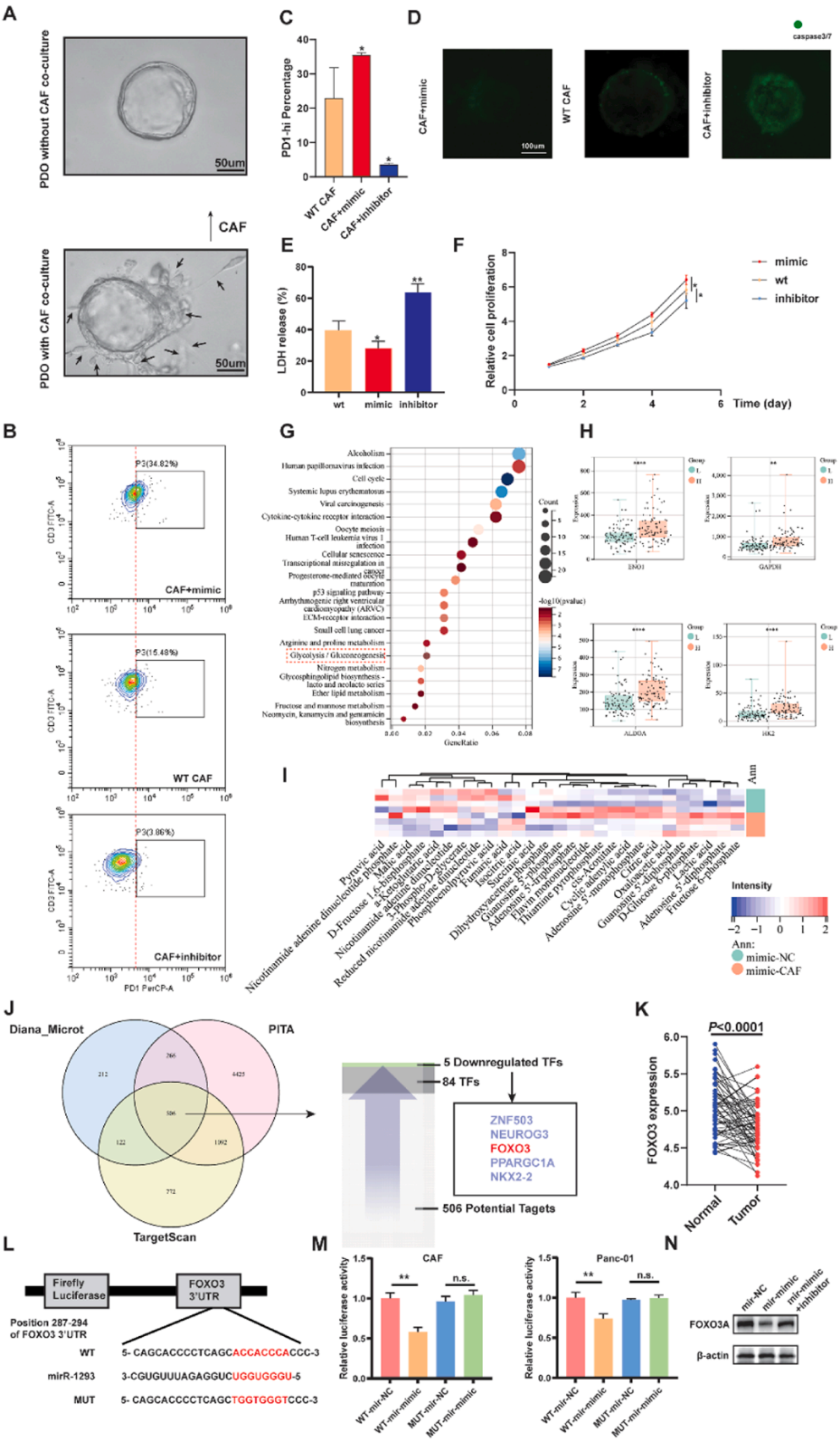

(caption on next page)

Fig. 6. Targeting miR-1293 may boost T cell-mediated anti-tumor immunity and prolonged prognosis in PDAC. (A) Representative microscopic picture for cocultured PDOs and CAFs (Bright field). (B-C) Transfection of CAFs with miR-1293 mimic and inhibitor affects PD-1 expression in co-cultured T cells (mean ± SD). (D) Inhibiting miR-1293 in CAFs enhances apoptosis in co-cultured PDOs under T cell assault. (E) T cells co-cultured with CAFs of varying transfections exhibit distinct cytotoxicity (mean ± SD). (F) miR-1293 expression in PDAC cells modestly influences cell proliferation (mean ± SD). (G) KEGG analysis unveiled dysregulation of genes associated with glycolysis/gluconeogenesis in correlation with miR-1293 levels. (H) In PDACs exhibiting high miR-1293 levels, four glycolytic genes exhibited upregulation. (I) Heatmap showed the differences of metabolites abundance between two groups with indicated treatment. (J-K) Integrated analysis identified FOXO3 as a potentially downregulated TF with a potential interaction with miR-1293 in PDACs. (L-M) The results of a luciferase reporter assay provided supporting evidence for the binding of miR-1293 to FOXO3 mRNA (mean ± SD). (N) Western blot analysis demonstrated that miR-1293 reduces the expression of FOXO3.

PLSDA revealed that the two groups exhibited distinct metabolic landscapes (Fig. S5A-B). These results provided robust support for the assertion that miR-1293 is intricately associated with the upregulation of glycolytic activity, such as lactic acid, which is the end product of glycolysis (Fig. S5C). Additionally, in the co-culture group with CAFs transfected with mimic-miR-1293, there is an elevation in the intensity of glucose-6-phosphate and a reduction in the intensity of malic acid, an intermediate product of the TCA cycle, which suggested the utilization of glucose, implying an upregulation in overall glucose utilization rate and a metabolic flux shifting towards glycolysis (Fig. S5D-E). In this particular context, we delved deeper into understanding how miR-1293 influences glycolysis. To begin, we initiated our investigation by analyzing the overlap of predicted downstream genes using data from three distinct databases. Subsequently, we honed our focus on transcription factors due to notable alterations observed in numerous enzymes within the glycolytic pathway at the transcriptome level. Out of the 506 potential downstream genes, a subset of 84 was identified as transcription factors. Moving forward, considering the well-established elevation of glycolytic activity in tumors and its positive correlation with miR-1293 upregulation, our objective was to pinpoint a transcription factor that experiences downregulation in PDAC. This narrowed our search down to just five final candidate transcription factors. Among these, only FOXO3 had previously been suggested to exhibit a negative association with glycolysis [3,4,47,7] (Fig. 6J). Meanwhile, FOXO3 expression was downregulated in PDAC (Fig. 6K). To authenticate the interaction between miR-1293 and FOXO3, we conducted experiments utilizing a luciferase reporter assay. Our findings indicate that miR-1293 can bind to the 3′UTR region of FOXO3 mRNA in both CAF and Panc-1 cells (Fig. 6L-M). Furthermore, mimic-miR-1293 resulted in a reduction in the protein levels of FOXO3, whereas the inhibitor-miR-1293 served to restore the expression of FOXO3 (Fig. 6N). In conclusion, miR-1293 may increase the accumulation of glycolytic products via FOXO3 inhibition, which ultimately fuels immune evasion in PDAC.

4.7. miR-1293 is a biomarker of unfavorable prognosis for PDAC

To validate the role of hsa-miR-1293 in PDAC progression in an in vivo context, we established a PDX model and introduced human PBMC into mice (Fig. 7A). We administered PBMC only seven days after xenograft transplantation, a regimen typically severely impedes tumor growth. As anticipated, xenografts comprised of a mixture of PDAC tissue and CAF-mimic-NC did not exhibit rapid growth in the subsequent 21-day observation period (Fig. 7B-C). In stark contrast, xenografts composed of PDAC tissue and CAF-mimic-miR-1293 displayed a significantly higher rate of proliferation (Fig. 7B-C). Employing flow cytometry to assess human CD3 + T cells, we observed a decreased abundance of human T cells in the group treated with CAF-mimic-miR-1293 compared to the group treated with CAF-mimic-NC (Fig. 7D), suggesting miR-1293 in CAF may impedes the recruitment of T cells. Next, we assessed miR-1293 expression using FISH in PDAC tissues. Compared to adjacent pancreatic tissue, miR-1293 expression was significantly elevated in cancerous regions ($P < 0.01$) (Fig. 7E-F). However, miR-1293 expression is irrelevant with tumor size (Fig. 7G). Furthermore, based on a PDAC cohort (Table S1), we examined the relationship between miR-1293 expression and patient prognosis. By conducting a log-rank test on follow-up data, we discovered that higher miR-1293 levels in pancreatic cancer tissues correlated with poorer prognosis (HR=1.53, $P = 0.01$) (Fig. 7H). This suggests that miR-1293 could serve as a potential biomarker indicating unfavorable outcomes for pancreatic cancer patients independent of tumor size.

5. Discussion

Exosomes have been recognized as essential regulators of miRNA transmission and communication between cells in tumor microenvironment. For instance, exosomes miRNA-301a, derived from hypoxic pancreatic cancer cells, have been found to induce M2 polarization of macrophages. This effect is attributed to the activation of the PTEN/PI3Kγ pathway [40]. Research conducted by Pang et al. demonstrated that pancreatic cancer cells produce and secrete miRNA-155 within exosomes, which functions to activate fibroblasts [27]. In this context, it is crucial to study the sources and destinations of exosome-miRNAs through high-throughput sequencing methods to understand the potential biological functions of these miRNAs. In the present study, we employed snRNA-seq and exosome-small RNA-seq techniques to explore the source of exosome miRNA and their downstream effects in PDAC microenvironment. Traditional scRNA-seq is not well-suited for combining with exosome small RNA-seq for several reasons. First, during tissue dissociation, cells retain metabolic activity and may release and absorb exocrine substances, particularly under strong external stimulation such as enzymolysis. This can greatly impact the accuracy and reliability of the sequenced data. Secondly, the enzymes used in the dissociation process can negatively affect exosomes, potentially causing the collapse of vesicle structures and making it difficult to purify high-quality exosomes. Moreover, the 37 ℃ enzymolysis environment might significantly affect the stability of RNA within the vesicles, even if the vesicle structures remain undamaged. To address these issues, our study employed snRNA-seq [6], which processes samples under low-temperature conditions, avoiding unnecessary RNA loss in exosomes.

Based on the pipeline, we constructed a novel intercellular communication network by integrating miRNA tracing and miRNA-target effects with ligand-receptor pair analysis, shedding light on the complex interplay between various cell types in the PDAC microenvironment. In addition, we uncovered a prognosis-relevant exosome miRNA, hsa-miR-1293, in the immune microenvironment of PDAC. Prior research has indicated that hsa-miR-1293 is overexpressed in hepatocellular cancer [48] and serves as an unfavorable prognostic factor for lung cancer [17]. On the contrary, hsa-miR-1293 was a tumor suppressive factor for renal cancer [20,22]. In this study, we discovered that high level of hsa-miR-1293 was associated with elevated MDSC levels, reduced CD8 + T cell infiltration, and poorer prognosis, suggesting a potential role for hsa-miR-1293 in modulating tumor immune evasion and reducing patient survival time. Furthermore, hsa-miR-1293 expression positively correlated with TMB, MSI, and neoantigen levels, indicating that inhibiting hsa-miR-1293 might enhance immunotherapy efficacy. The in-vitro co-culture system and in-vivo preclinical experiments employed in our research further showed that targeting hsa-miR-1293 could improve T cell-mediated anti-tumor immunity and may prolong patients' OS, offering a potential therapeutic strategy for PDAC.

Although the present study provides valuable insights into the role of miRNAs in the PDAC microenvironment, there are some limitations to consider. On one hand, the present analysis was mainly based on

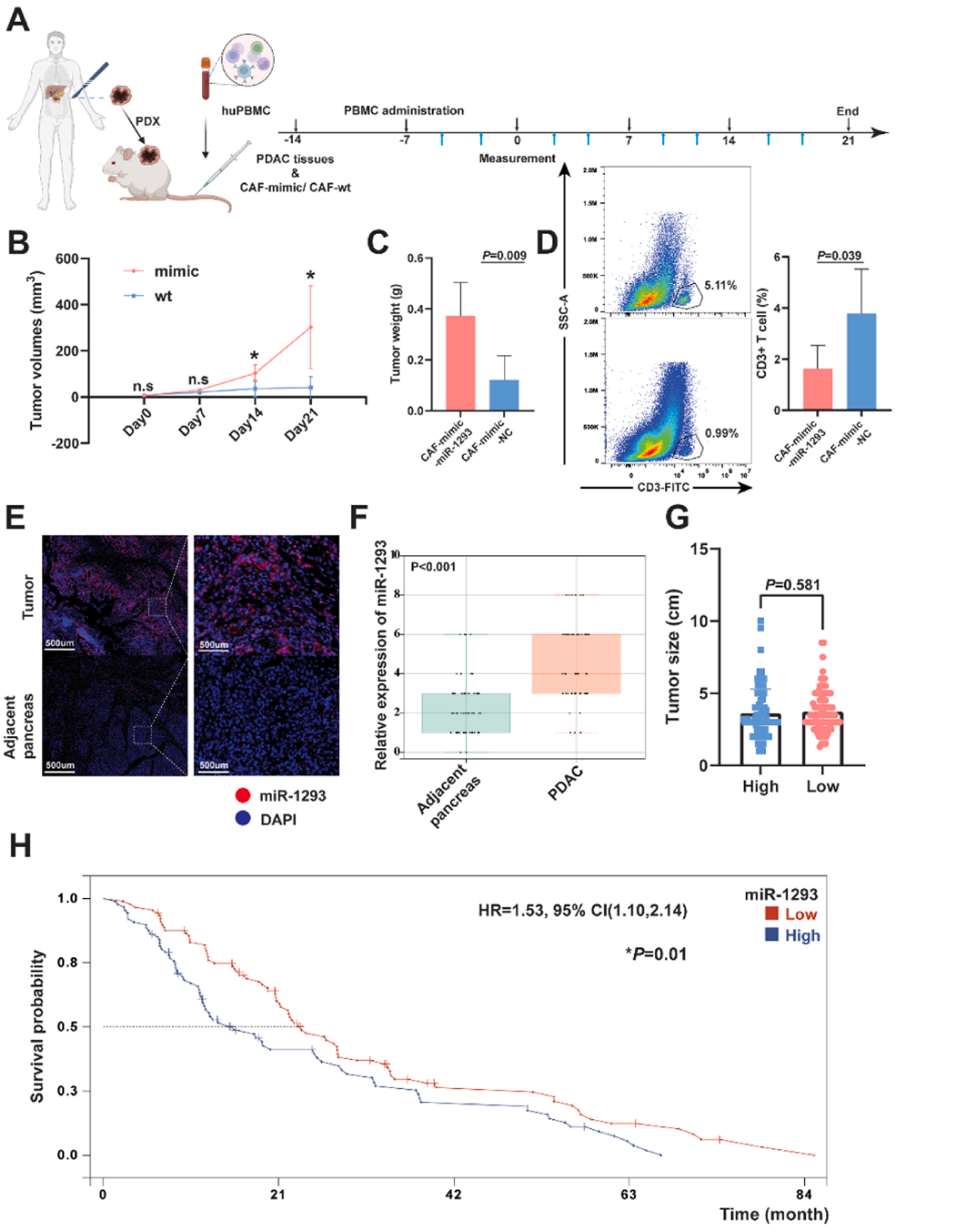

Fig. 7. miR1293 serves as a biomarker for unfavorable prognosis in PDAC. (A) Timeline for in vivo experiments: Blue arrows represent intraperitoneal administration of Durvalumab at a dose of 0.5 mg/kg twice a week to mice. (B-C) Growth curve and measurement of tumor weight in the group treated with CAF-mimic-miR-1293 and the group treated with CAF-mimic-NC (n = 5) (mean ± SD). (D) Reduced infiltration of CD3 + T cells in the group treated with CAF-mimic-miR-1293. (E-F) miR-1293 exhibits substantial upregulation in pancreatic cancer tissues compared to adjacent pancreatic tissues. (G) Tumor size showed no differences between miR-1293-high and miR-1293-low pancreatic cancer samples (N = 57) (mean ± SD). (H) PDAC patients with elevated miR-1293 expression are associated with poorer prognoses (N = 176).

computational prediction and in silico analyses, warranting further experimental validation to confirm the identified miRNA-target interactions and their functional consequences. In this study, we exemplified the immunosuppressive role of miR-1293 in PDAC. On the other hand, the relatively small sample size of PDAC tissues used in this study may limit the generalizability of our findings. Owing to the limited cell number and the characteristics of snRNA-seq discussed in the previous section, we were unable to comprehensively identify all cell subtypes in this study. Consequently, the exosome miRNA information for some cell types with limited proportions may have been overlooked, such as endocrine cells. Nevertheless, our study serves as a paradigm for future research to design large-scale experiments on conducting snRNA-seq and exosome small RNA sequencing using a single bulk of tissue. Lastly, the role of miRNAs in modulating the immune microenvironment is undoubtedly complex, and our study only explored a limited number of miRNAs and their potential targets.

In conclusion, our study presents a workflow using human PDAC tissues that enables the construction of a cell-cell communication network based on snRNA-seq, exosome-miRNA detection, and ligand-receptor analysis. Further experimental validation and functional studies are anticipated to uncover and confirm the therapeutic potential of identified miRNAs as biomarkers, which could be translated into clinical applications and benefit patients with cancer.

Ethics approval

PDAC tissues were collected in FUSCC and was approved by the Clinical Research Ethics Committee of FUSCC. Specimens were collected upon informed consent of patients with PDAC.

Funding

This study was jointly supported by the National Natural Science Foundation of China (U21A20374), Shanghai Municipal Science and Technology Major Project (21JC1401500), Scientific Innovation Project of Shanghai Education Committee (2019-01-07-00-07-E00057), Clinical Research Plan of Shanghai Hospital Development Center (SHDC2020CR1006A), Shanghai Rising-Star Program (20QA1402100) and Xuhui District Artificial Intelligence Medical Hospital Cooperation Project (2021–011).

CRediT authorship contribution statement

Jin Xu: Investigation. **Wei Wang:** Methodology. **Qingcai Meng:** Conceptualization. **Yuan Liu:** Investigation, Validation. **Qiong Du:** Supervision, Validation. **Chen Liang:** Investigation, Methodology. **Jie Hua:** Conceptualization, Data curation. **Bo Zhang:** Investigation. **Xianjun Yu:** Conceptualization. **Si Shi:** Conceptualization, Data curation. **Rong Tang:** Conceptualization, Formal analysis, Methodology, Writing – original draft, Writing – review & editing. **Zifeng zhang:** Data curation, Formal analysis, Methodology.

Declaration of Competing Interest

The authors declare that they have no known competing financial interests or personal relationships that could have appeared to influence the work reported in this paper.

Data availability

The datasets used and/or analyzed during the current study are available from the corresponding author on reasonable request.

Acknowledgements

We express our gratitude to Siyu Tong of Oebiotch for her valuable assistance in annotating pre-miRNAs for the snRNA data and for her contributions to other bioinformatic tasks.

Consent for publication

All authors are consent for publication.

Appendix A. Supporting information

Supplementary data associated with this article can be found in the online version at doi:10.1016/j.csbj.2024.04.021.

References

[1] AlMusawi S, Ahmed M, Nateri AS. Understanding cell-cell communication and signaling in the colorectal cancer microenvironment. Clin Transl Med 2021;11:e308.
[2] Bridges K, Miller-Jensen K. Mapping and validation of scRNA-seq-derived cell-cell communication networks in the tumor microenvironment. Front Immunol 2022;13:885267.
[3] Chen W, Jiang J, Gong L, Shu Z, Xiang D, Zhang X, et al. Hepatitis B virus P protein initiates glycolytic bypass in HBV-related hepatocellular carcinoma via a FOXO3/miRNA-30b-5p/MINPP1 axis. J Exp Clin Cancer Res 2021;40:1 (CR).
[4] Chu Z, Huo N, Zhu X, Liu H, Cong R, Ma L, et al. FOXO3A-induced LINC00926 suppresses breast tumor growth and metastasis through inhibition of PGK1-mediated Warburg effect. Mol Ther: J Am Soc Gene Ther 2021;29:2737–53.
[5] Cristescu R, Mogg R, Ayers M, Albright A, Murphy E, Yearley J, et al. Pan-tumor genomic biomarkers for PD-1 checkpoint blockade-based immunotherapy. Science 2018;362.
[6] Ding J, Adiconis X, Simmons SK, Kowalczyk MS, Hession CC, Marjanovic ND, et al. Systematic comparison of single-cell and single-nucleus RNA-sequencing methods. Nat Biotechnol 2020;38:737–46.
[7] Dong Z, Yang J, Li L, Tan L, Shi P, Zhang J, et al. FOXO3a-SIRT6 axis suppresses aerobic glycolysis in melanoma. Int J Oncol 2020;56:728–42.
[8] Driehuis E, Kretzschmar K, Clevers H. Establishment of patient-derived cancer organoids for drug-screening applications. Nat Protoc 2020;15:3380–409.
[9] Garcia-Martin R, Wang G, Brandão BB, Zanotto TM, Shah S, Kumar Patel S, et al. MicroRNA sequence codes for small extracellular vesicle release and cellular retention. Nature 2022;601:446–51.
[10] Jin S, Guerrero-Juarez CF, Zhang L, Chang I, Ramos R, Kuan CH, et al. Inference and analysis of cell-cell communication using CellChat. Nat Commun 2021;12:1088.
[11] Jing R, Zhong QQ, Long TY, Pan W, Qian ZX. Downregulated miRNA-26a-5p induces the apoptosis of endothelial cells in coronary heart disease by inhibiting PI3K/AKT pathway. Eur Rev Med Pharmacol Sci 2019;23:4940–7.
[12] Kalluri R, LeBleu VS. The biology, function, and biomedical applications of exosomes. Science 2020;367.
[13] Koikawa K, Kibe S, Suizu F, Sekino N, Kim N, Manz TD, et al. Targeting Pin1 renders pancreatic cancer eradicable by synergizing with immunochemotherapy. Cell 2021;184:4753–71. e4727.
[14] Kumar MP, Du J, Lagoudas G, Jiao Y, Sawyer A, Drummond DC, et al. Analysis of single-cell RNA-Seq identifies cell-cell communication associated with tumor characteristics. Cell Rep 2018;25:1458–68. e1454.
[15] Lee YS, Dutta A. MicroRNAs in cancer. Annu Rev Pathol 2009;4:199–227.
[16] Lei Y, Tang R, Xu J, Wang W, Zhang B, Liu J, et al. Applications of single-cell sequencing in cancer research: progress and perspectives. J Hematol Oncol 2021;14:91.
[17] Li J, Gu X, Gao C, Zhang J. Six MicroRNA prognostic models for overall survival of lung adenocarcinoma. Genet Res 2022;2022:5955052.
[18] Liang C, Shi S, Qin Y, Meng Q, Hua J, Hu Q, et al. Localisation of PGK1 determines metabolic phenotype to balance metastasis and proliferation in patients with SMAD4-negative pancreatic cancer. Gut 2020;69:888–900.
[19] Liu X, Tang R, Xu J, Tan Z, Liang C, Meng Q, et al. CRIP1 fosters MDSC trafficking and resets tumour microenvironment via facilitating NF-κB/p65 nuclear translocation in pancreatic ductal adenocarcinoma. Gut 2023.
[20] Liu XL, Pan WG, Li KL, Mao YJ, Liu SD, Zhang RM. miR-1293 suppresses tumor malignancy by targeting hydrocyanic oxidase 2: therapeutic potential of a miR-1293/Hydrocyanic oxidase 2 axis in renal cell carcinoma. Cancer biotherapy Radiopharm 2020;35:377–86.
[21] Lu Y, Thavarajah T, Gu W, Cai J, Xu Q. Impact of miRNA in atherosclerosis. Arterioscler, Thromb, Vasc Biol 2018;38:e159–70.
[22] Luo W, Wang L, Luo MH, Huang YZ, Yang H, Zhou Y, et al. hsa-mir-3199-2 and hsa-mir-1293 as Novel Prognostic Biomarkers of Papillary Renal Cell Carcinoma by COX Ratio Risk Regression Model Screening. J Cell Biochem 2017;118:3488–94.
[23] Mao X, Xu J, Wang W, Liang C, Hua J, Liu J, et al. Crosstalk between cancer-associated fibroblasts and immune cells in the tumor microenvironment: new findings and future perspectives. Mol Cancer 2021;20:131.
[24] Mashouri L, Yousefi H, Aref AR, Ahadi AM, Molaei F, Alahari SK. Exosomes: composition, biogenesis, and mechanisms in cancer metastasis and drug resistance. Mol Cancer 2019;18:75.

[25] McCann JV, Xiao L, Kim DJ, Khan OF, Kowalski PS, Anderson DG, et al. Endothelial miR-30c suppresses tumor growth via inhibition of TGF-β-induced Serpine1. J Clin Investig 2019;129:1654–70.
[26] Orso F, Quirico L, Dettori D, Coppo R, Virga F, Ferreira LC, et al. Role of miRNAs in tumor and endothelial cell interactions during tumor progression. Semin Cancer Biol 2020;60:214–24.
[27] Pang W, Su J, Wang Y, Feng H, Dai X, Yuan Y, et al. Pancreatic cancer-secreted miR-155 implicates in the conversion from normal fibroblasts to cancer-associated fibroblasts. Cancer Sci 2015;106:1362–9.
[28] Qi R, Bai Y, Li K, Liu N, Xu Y, Dal E, et al. Cancer-associated fibroblasts suppress ferroptosis and induce gemcitabine resistance in pancreatic cancer cells by secreting exosome-derived ACSL4-targeting miRNAs. Drug Resist Update: Rev Comment Antimicrob Anticancer Chemother 2023;68:100960.
[29] Rizzo A, Ricci AD, Brandi G. PD-L1, TMB, MSI, and other predictors of response to immune checkpoint inhibitors in biliary tract cancer. Cancers 2021;13.
[30] Rong Z, Shi S, Tan Z, Xu J, Meng Q, Hua J, et al. Circular RNA CircEYA3 induces energy production to promote pancreatic ductal adenocarcinoma progression through the miR-1294/c-Myc axis. Mol Cancer 2021;20:106.
[31] Rupaimoole R, Slack FJ. MicroRNA therapeutics: towards a new era for the management of cancer and other diseases. Nat Rev Drug Discov 2017;16:203–22.
[32] Shi Y, Gao W, Lytle NK, Huang P, Yuan X, Dann AM, et al. Targeting LIF-mediated paracrine interaction for pancreatic cancer therapy and monitoring. Nature 2019; 569:131–5.
[33] Shorning BY, Dass MS, Smalley MJ, Pearson HB. The PI3K-AKT-mTOR pathway and prostate cancer: at the crossroads of AR, MAPK, and WNT Signaling. Int J Mol Sci 2020;21.
[34] Siegel RL, Miller KD, Fuchs HE, Jemal A. Cancer Statistics, 2021. CA: a Cancer J Clin 2021;71:7–33.
[35] Stefani C, Miricescu D, Stanescu S, II, Nica RI, Greabu M, Totan AR, et al. Growth Factors, PI3K/AKT/mTOR and MAPK Signaling Pathways in Colorectal Cancer Pathogenesis: Where Are We Now? Int J Mol Sci 2021;22.
[36] Su L, Zhang J, Zhang X, Zheng L, Zhu Z. Identification of cell cycle as the critical pathway modulated by exosome-derived microRNAs in gallbladder carcinoma. Med Oncol (North, Lond, Engl) 2021;38:141.
[37] Su M, Pan T, Chen QZ, Zhou WW, Gong Y, Xu G, et al. Data analysis guidelines for single-cell RNA-seq in biomedical studies and clinical applications. Mil Med Res 2022;9:68.
[38] Tang R, Liu X, Wang W, Hua J, Xu J, Liang C, et al. Identification of the Roles of a Stemness Index Based on mRNA expression in the prognosis and metabolic reprograming of pancreatic ductal adenocarcinoma. Front Oncol 2021;11:643465.
[39] Tang R, Xu J, Wang W, Meng Q, Shao C, Zhang Y, et al. Targeting neoadjuvant chemotherapy-induced metabolic reprogramming in pancreatic cancer promotes anti-tumor immunity and chemo-response. Cell Rep Med 2023;4:101234.
[40] Wang X, Luo G, Zhang K, Cao J, Huang C, Jiang T, et al. Hypoxic tumor-derived exosomal miR-301a Mediates M2 macrophage polarization via PTEN/PI3Kγ to promote pancreatic cancer metastasis. Cancer Res 2018;78:4586–98.
[41] Weiss F, Lauffenburger D, Friedl P. Towards targeting of shared mechanisms of cancer metastasis and therapy resistance. Nat Rev Cancer 2022;22:157–73.
[42] Xiao FJ, Zhang D, Wu Y, Jia QH, Zhang L, Li YX, et al. miRNA-17-92 protects endothelial cells from erastin-induced ferroptosis through targeting the A20-ACSL4 axis. Biochem Biophys Res Commun 2019;515:448–54.
[43] Yokota Y, Noda T, Okumura Y, Kobayashi S, Iwagami Y, Yamada D, et al. Serum exosomal miR-638 is a prognostic marker of HCC via downregulation of VE-cadherin and ZO-1 of endothelial cells. Cancer Sci 2021;112:1275–88.
[44] Zhang BY, Han L, Tang YF, Zhang GX, Fan XL, Zhang JJ, et al. METTL14 regulates M6A methylation-modified primary miR-19a to promote cardiovascular endothelial cell proliferation and invasion. Eur Rev Med Pharmacol Sci 2020;24: 7015–23.
[45] Zhang H, Deng T, Liu R, Ning T, Yang H, Liu D, et al. CAF secreted miR-522 suppresses ferroptosis and promotes acquired chemo-resistance in gastric cancer. Mol Cancer 2020;19:43.
[46] Zhang Z, Richmond A, Yan C. Immunomodulatory Properties of PI3K/AKT/mTOR and MAPK/MEK/ERK inhibition augment response to immune checkpoint blockade in melanoma and triple-negative breast cancer. Int J Mol Sci 2022;23.
[47] Zhou K, Wei Y, Li X, Yang X. MiR-223-3p targets FOXO3a to inhibit radiosensitivity in prostate cancer by activating glycolysis. Life Sci 2021;282:119798.
[48] Zhu B, Gu S, Wu X, He W, Zhou H. Bioinformatics analysis of tumor-educated platelet microRNAs in patients with hepatocellular carcinoma. Biosci Rep 2021;41.